Estimation of woodland canopy structure with terrestrial LiDAR: expanded methods

John L. Godlee

Contents

1 Introduction

This document provides detailed field and analytical methods for the study of tree canopy structure in southern African woodlands. The study aimed to understand the effects of tree species diversity and composition on tree canopy structure and grassy biomass. Chapter XXX contains the same methods in brief.

2 Sampling

Fieldwork was conducted at two sites, the first in Bicuar National Park, southwest Angola (S15.1°, E14.8°), and the second in and around Mtarure Forest Reserve, southeast Tanzania (S9.0°, E39.0°). Fieldwork was conducted during the peak growth period of each site, in order to capture the highest foliage volume in the canopy and the largest grass volume in the understorey.

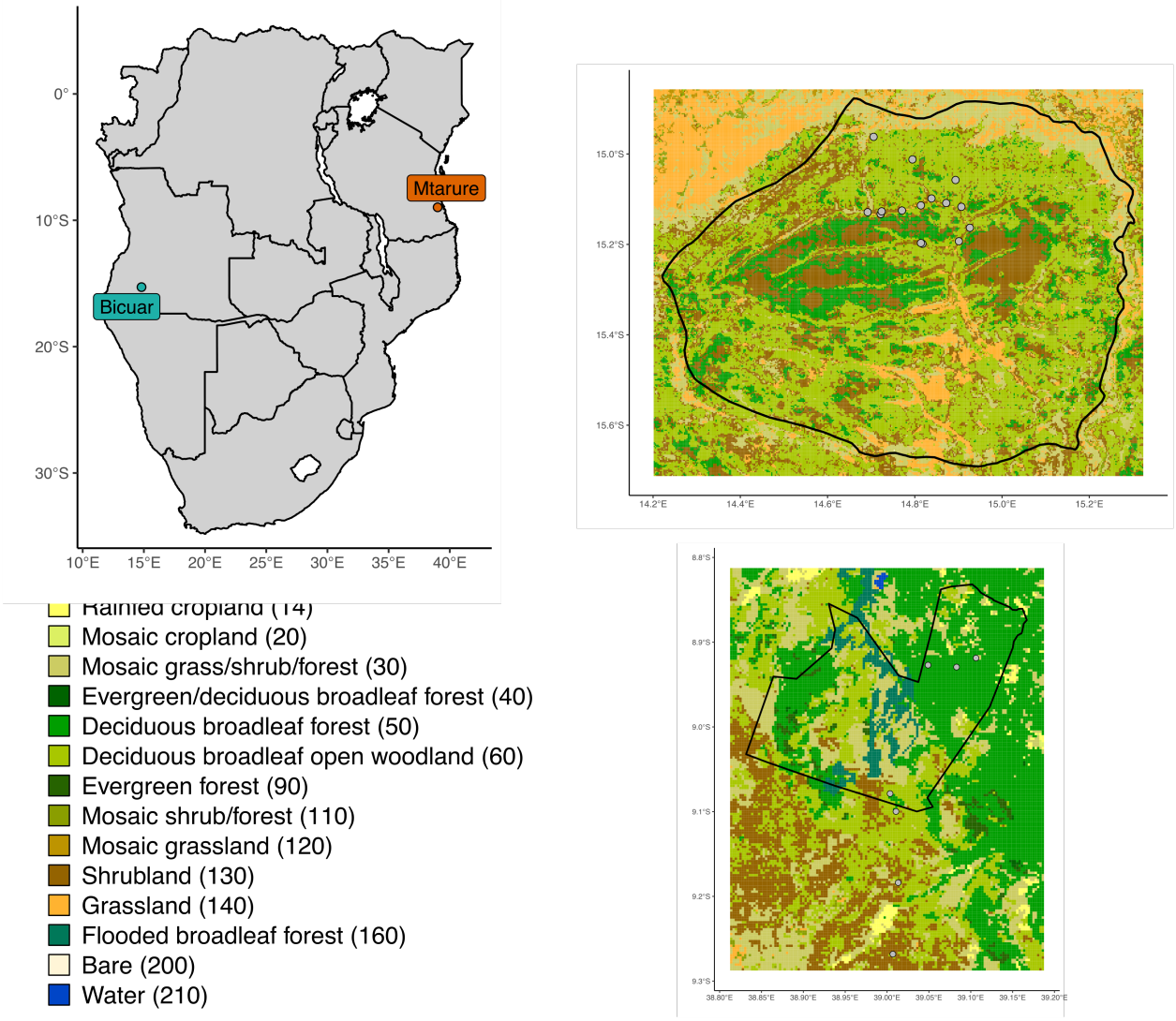

Figure 1: Location of study sites within southern Africa (a), and of 1 ha plots within each site. The blue polygons denote the boundaries of protected areas which encompass the majority of study sites, Bicuar National Park in Angola (b), and Mtarure Forest Reserve in Tanzania (c).

Site	MAT (°C)	MAP (mm y^{-1})	Temp. range (°C)	CWD (mm y^{-1})
Bicuar	20.8 (0.70)	825.9 (52.01)	24.5 (0.90)	-844.8 (44.29)
Mtarure	25.7 (0.24)	958.4 (25.19)	12.0 (0.33)	-739.6 (8.06)

Table 1: Climatic data for each site, extracted from WorldClim at 2.5 minute resolution. Values are the mean and standard deviation (in brackets) of all pixels intersecting each protected area. MAT = Mean Annual Temperature. MAP = Mean Annual Precipitation. Temp. range = Temperature range, calculated as the mean of annual difference between highest temperature of hottest month and lowest temperature of coldest month. CWD = Climatic Water Deficit, calculated as the sum of the difference between monthly rainfall and monthly evapotranspiration when the difference is negative, sensu Chave et al. (2014).

At each site, 1 ha permanent plots were sampled. In Angola, 15 plots were sampled, while in Tanzania, only seven were sampled, following the curtailment of fieldwork due to COVID-19 travel restrictions. Permanent plots were located in areas of homogeneous vegetation type, away from roads and undisturbed by humans, following the SEOSAW protocol (version 3.0, **SEOSAW_manual**). Plots were located quasi-randomly by first locating areas from satellite imagery expected to comprise savanna woodland vegetation. At each site, plots were deliberately located along a gradient of stem density.

Each permanent plot was further subdivided into nine 10 m diameter circular subplots arranged in a regular grid, with a buffer from the plot edge (Figure 2).

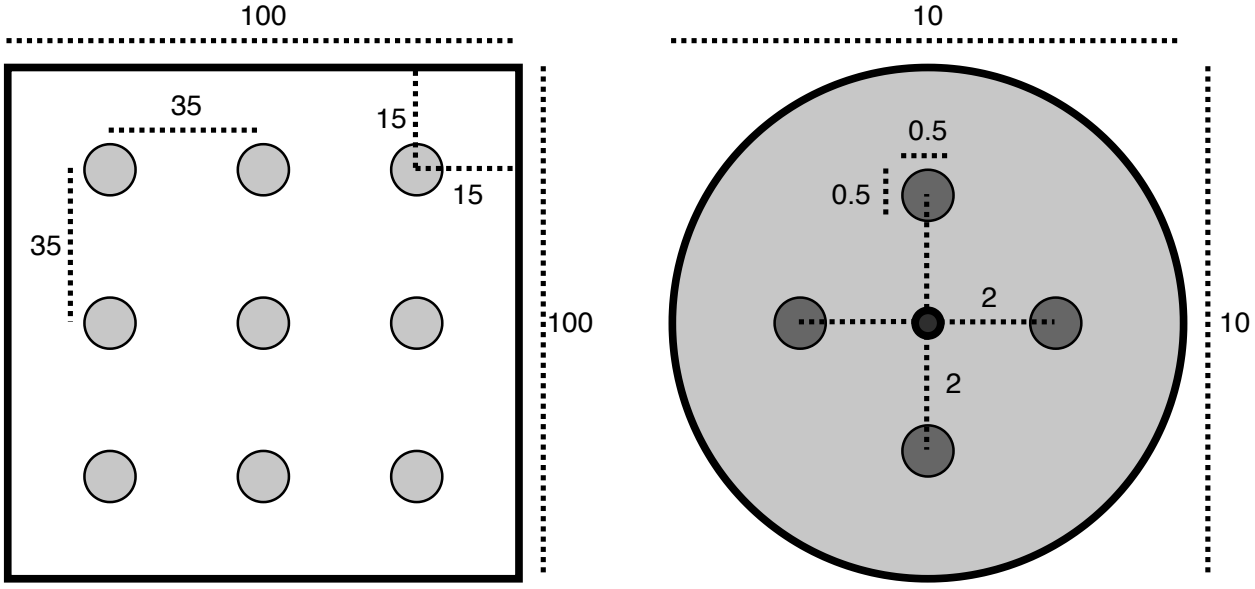

Figure 2: The layout of 10 m diameter subplots within each 1 ha square plot. Each subplot is situated inside a 15 m buffer from the plot edge, with 35 m between subplot centres. Subplots are arranged in a 3x3 grid. Disc-pasture measurements and biomass samples are located in cardinal directions 2 m from the centre of the subplot. All distances are in metres.

3 Field measurements

3.1 Trees

For each subplot, we measured all woody stems >5 cm trunk diameter with canopy material inside the subplot. For each stem we measured:

- Tree identity
- Trunk diameter (Diameter at breast height - 1.3 m)

For each tree, which may be composed of multiple stems, we measured:

- Species
- Height to top of canopy
- Canopy area, ellipse from two perpendicular measurements (Figure 3)
- Distance from subplot centre
- Compass direction from subplot centre

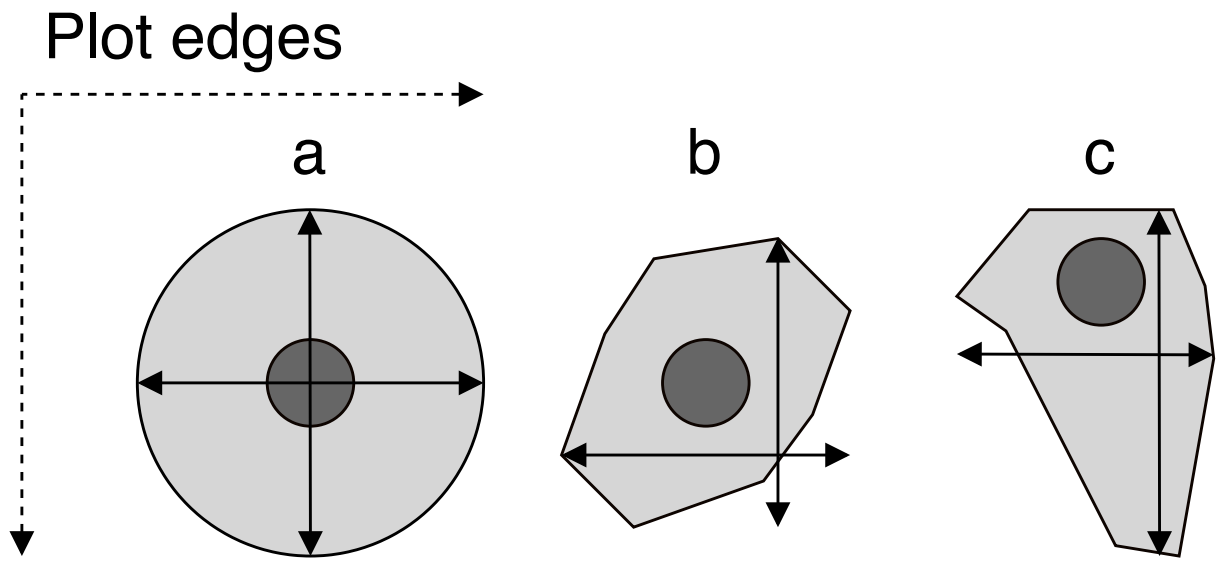

Figure 3: Examples of tree crowns as viewed from above to demonstrate how crown extent measurements are located. Darker grey circles show the main trunk. Extent measurements are taken parallel to the plot edge. a) shows a perfectly circular tree crown, b) and c) show irregular tree crowns, demonstrating that maximum crown extent in a given orientation be offset from the trunk.

3.2 Grassy biomass

Grassy volume and biomass within each subplot was estimated from four sample points located 2 m from the subplot centre in cardinal directions (Figure 2). At each point, a disc-pasture meter

measurement was taken with a 45.8 cm radius disc weighing exactly 1.5 kg (Bransby and Tainton, 1977). Small woody stems were removed from disc-pasture sample points before the disc-pasture measurement was taken. The location of the sample point was moved if the designated point intersected with coarse woody debris, rocks, immovable shrubs, or standing trees. Within each 1 ha plot, biomass harvesting was conducted at nine randomly allocated disc-pasture sample points. Tree leaf litter was removed from biomass samples. Grass samples in Angola were dried until the mass remained constant (±5 g) for >48 hours, then weighed to ascertain the grassy biomass. Grass samples from Tanzania could not be processed due to curtailment of fieldwork due to COVID-19 travel restrictions.

3.3 Hemispherical photography

At the centre of each subplot a single photograph was taken with a Nikon D750 full-frame DSLR camera, with a circular fisheye lens. The lens had an equisolid (equal area) projection, which avoids image distortion. The projection function is given by:

$$R = 2f \sin(\theta/2) \tag{1}$$

Where R is the radial position of a point on the image on the sensor, f is the focal length of the lens, and θ is the angle in radians of the desired angular radius of the cropped image.

The photo was taken facing directly to zenith, with the top of the camera facing to magnetic north, at a height of 1.3 m or above understorey vegetation, whichever was higher. Table 2 shows describes the camera settings for each hemispherical photo:

Table 2: Description of camera settings used for each hemispherical photo. Note that the values of shutter speed and ISO are deliberately variable within sensible thresholds to adapt to light conditions.

Setting	Value
Camera model	Nikon D750
Lens model	Sigma 8 mm f/3.5 EX DG Circular Fisheye
Pixel pitch	5.95 µm
Sensor resolution	24.3 MP
Shutter speed	>1/60s
Aperture	5-7
ISO	100-200
Exposure compensation	-0.7 (Brusa and Bunker, 2014)
Focus	∞ (Hu and Zhu, 2009; Frazer et al., 2001)
Image size	Large Fine JPEG - circular image 4016x4016 px
Orientation	Landscape

Photos were captured under uniform light conditions as much as possible, either under overcast skies or early in the day before direct sunlight could be seen on the photo.

ImageJ (Fiji version 2.1.0/1.53c) was used to binarize hemispherical photos (). We first split each image into red, green and blue channels. We used the Huang algorithm to automatically threshold images to separate sky from plant material, using the blue channel only, under the assumption that plant material reflects little blue light, while the sky reflects much more (). Images were saved as PNG at the original pixel resolution.

3.4 Stand structure

From the stem measurements we calculated a number of indices to characterise whole-plot and subplot stand structure.

We calculated the spatial mingling index (M) according to von Gadow and Hui (2002) at the plot level. The spatial mingling index is a spatially explicit estimate of the degree to which species are spatially mixed within a plot:

$$M = \sum_{i=1}^{N} (S_i / S \frac{1}{k} \sum_{j=1}^{k} v_j) \tag{2}$$

$$\text{with } v_j = \begin{cases} 0, & \text{neighbour } j \text{ same species as reference } i \\ 1, & \text{otherwise} \end{cases} \tag{3}$$

$$\tag{4}$$

where k is the number of nearest neighbours considered for each reference tree, S_i is the number of species found among the k nearest neighbours, S is the total number of species in the plot, and N is the total number of trees in the plot. In our case we used the conventional value of $k = 4$.

We also calculated the Winkelmass W according to von Gadow and Hui (2002) at the plot level. The Winkelmass estimates the degree of spatial uniformity in stem spatial distribution:

$$W = \sum_{i=1}^{N} \frac{1}{k} \sum_{j=1}^{k} v_j \tag{5}$$

$$\text{with } v_j = \begin{cases} 0, & \alpha_j \leq \alpha_0 \\ 1, & \text{otherwise} \end{cases} \tag{6}$$

$$\tag{7}$$

To estimate stand spatial structure in subplots we used an adapted version of the point density index (SC) *sensu* Spurr (1962):

$$SC = \sum_{k=1}^{n} [\frac{1}{4}(k - 0.5)(D_k / L_k)^2] / k \tag{8}$$

where k is the rank of the kth neighbour by stem diameter, D_k is the diameter of the kth neighbour , L_k is the distance from the subplot centre of the kth neighbour. For each subplot we defined the neighbourhood as all trees with canopy material inside the subplot boundary.

4 Terrestrial LIDAR

Within each subplot, a variable number of scans were recorded using a Leica HDS6100 phase-shift terrestrial laser scanner (TLS). The number and position of scans within a subplot was determined by the arrangement and density of canopy material in the subplot. Scan positions were arranged to minimise shadows within the canopy, and to maximise canopy penetration. Number of scans per subplot ranged between one and five in both Angola and Tanzania (Table 3).

Five Leica 6" planar tilt and turn targets were used at each subplot to align scans. To allow registration of scans among subplots, the location of each target was registered using a Leica VIVA GS10 GNSS unit, set up in post-processed kinematic (PPK) configuration with a base-station located ~100 m from the edge of each 1 ha plot. The location of each target was measured for at least 4 minutes. Further, we used the TrimbleRTX GNSS post-processing service to precisely locate each target (Chen et al., 2011). When registering scans we discarded targets with location accuracy of >3 cm.

Table 3: Description of scan settings used for each scan.

Setting	Value
Scanner model	Leica HDS6100
Wavelength	650-690 nm
Spot size at exit	3 mm
Beam divergence	0.22 mrad
Range	79 m @90%; 50 m @18% albedo
Azimuth range	0-360°
Zenith range	0-155°
Increments	0.018°
Point spacing over 25 m	7.9 mm
Pixels per line	20000
Lines	10000
Compressed file size	~800 MB
Duration of scan	6 minutes 44 seconds

4.1 Registration

Scan registration for each subplot was conducted in Leica Cyclone (version 9.1). Targets from each scan were aligned using Cyclone's automatic target acquisition.

After registration, scan scenes were exported from Cyclone as PTX files, one per subplot.

4.2 Voxelisation

PTX files were converted to compressed LAZ files using PDAL (). The exact code used to extract and apply the PTX rotation matrix to each point in the PTX file can be found IN THIS APPENDIX HERE.

LAZ files were voxelised to different voxel sizes depending on the application of the data. For grassy biomass estimation, we used 2 cm^3 cubic voxels, while for subplot height profile estimation we used 5 cm^3 voxels, and for whole plot canopy rugosity we used 10 cm^3 voxels. WHY THO

4.3 Noise reduction

Outlier detection and noise reduction was conducted in PDAL using the `filters.outlier` filter, using the "statistical method" (sensu Rusu et al. 2008), with $k = 8$ (mean number of neighbours), and $m = 1.96$ (standard deviation threshold, approximating a 95% confidence interval):

$$\overline{\mu} = \frac{1}{N}\sum_{i=1}^{N}\mu_i \tag{9}$$

$$\sigma = \sqrt{\frac{1}{N-1}\sum_{i=1}^{N}(\mu_i - \overline{\mu})^2} \tag{10}$$

$$t = \mu + m\sigma \tag{11}$$

$$\text{outlier}_i = \begin{cases} \text{true}, & \text{if } \mu_i >= t \\ \text{false}, & \text{otherwise} \end{cases} \tag{12}$$

where N is the number of points in the scene, $\overline{\mu}$ is the mean distance to nearest neighbour points, and σ is the standard deviation of these distances. t is the threshold distance used to define an outlier.

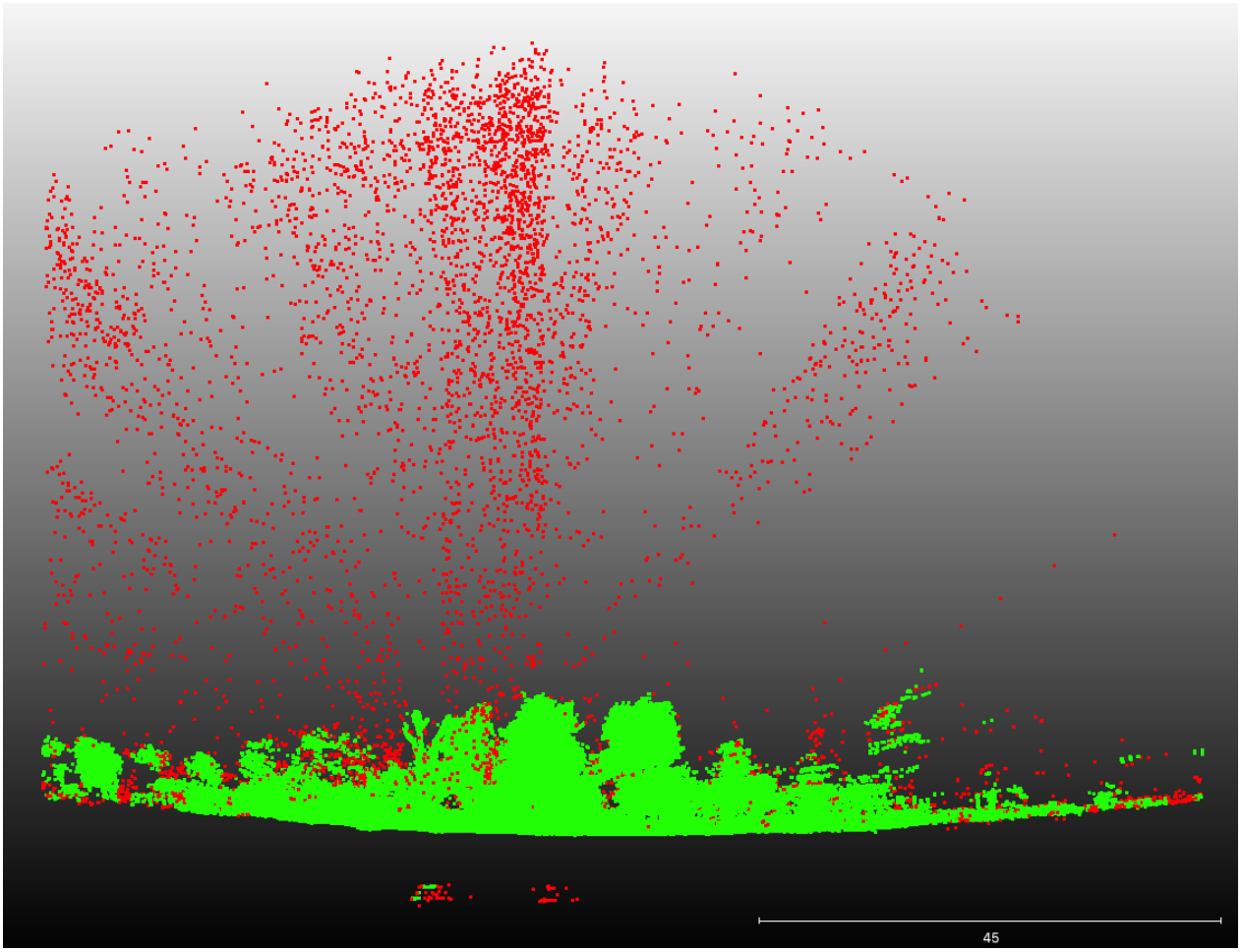

Figure 4: 2 m deep cross section of subplot showing the efficacy of the noise reduction and voxelisation process. Red points are points excluded by this cleaning process, while green points are used in further analysis.

4.4 LiDAR analysis

4.4.1 Foliage density profiles

To estimate subplot foliage density profiles, first the point cloud was cropped to a 10 m diameter cylinder of infinite height. Then the `filters.pmf` (Progressive Morphological Filter - PMF) PDAL function was used to identify ground points (sensu Zhang et al. 2003). The `filters.hag_nn` (Nearest Neighbour) PDAL function was used to generate height above ground of each point within the cylinder. Points below ground level were then discarded. Height profile points were exported to a XYZ file then imported into R for further processing.

We excluded points above the 99.9th percentile of height, under the assumption that these often constituted noise that had not been adequately removed by PDAL.

In R, within each 5 cm width vertical layer, we calculated the gap fraction as the proportion of unfilled 5 cm^3 voxels. We filtered the point cloud data to the tree canopy, excluding grass. We identified the breakpoint between the grassy understorey and the tree canopy as the first local minima above 1.3 m from the ground.

We extracted statistics from the foliage density profile for use in statistical analysis. We first smoothed the density profile using a loess model with a span of 0.1. We then calculated the number of local maxima and minima along the profile. We defined local maxima and minima as points where the gap fraction of the surrounding 50 cm of 5 cm bins was lower or higher, respectively.

We calculated the effective number of layers (ENL), using the true-numbers equivalent of the Shannon diversity index (sensu (Ehbrecht et al., 2016)). We also calculated the conventional Shannon diversity index on the gap fraction of 50 cm bins:

$$H' = -\sum_{i=1}^{N} p_i \ln p_i \tag{13}$$

Where N is the number of 50 cm bins in the height profile, and p_i is the proportion of filled voxels in layer i (gap fraction).

We calculated the area under the curve of foliage density using trapezoid estimation.

We extracted the height of the maximum foliage density peak, and calculated the difference between the highest and lowest local maxima. We also extracted the maximum canopy height within the subplot.

We calculated the coefficient of variation of the point cloud height distribution.

To describe the uniformity of the foliage density distribution we used Ripley's L function, which is more commonly used in describing spatial variation across a 2 dimensional surface. Ripley's L is an adjustment to Ripley's K, defined as:

$$\widehat{K}(t) = \lambda^{-1} \sum_{i \neq j} \frac{I(d_{ij} < t)}{n} \tag{14}$$

$$\widehat{L}(t) = \left(\frac{\widehat{K}(t)}{\pi} \right)^{1/2} \tag{15}$$

We also used the standard error of a linear model of foliage density and height as a simple single number method of describing the uniformity of foliage density.

4.4.2 Canopy gap fraction

Due to terrestrial LiDAR measurement locations being spread over the subplot to avoid occlusion of canopy material, we simulated a scan position at the centre of the subplot using the point cloud data from all scans per subplot. Similar to the processing chain for the foliage density profiles, PDAL was used to crop the point cloud to a 20 m cylinder around the subplot centre, then used `filters.hag_nn` to classify ground points and recalculate height above ground. We cropped the point cloud to points above 1.3 m, with a 50 cm exclusion sphere around the scan position at 1.3 m above the ground. The point cloud was converted to a POV-Ray object, where each point was transformed to a 1 cm^3 cube. POV-Ray was then used to produce a ray-traced image. As with the hemispherical photos, we used a fisheye lens with an equisolid projection and a view angle of 180°, located at the subplot centre, at the same height as the hemispherical photo, with the top

of the camera facing magnetic north and the camera facing straight up. Each cube was set as a non-reflective object, and the sky had an equal gamma of 1.0. POV-Ray produced an image of 4016x4016 px, identical to the cropped circular dimensions of the images produced by the hemispherical photos.

Simple canopy gap fraction as seen from the ground was measured using two methods: 1) hemispherical photography and 2) terrestrial LiDAR. Hemiphot () was used to estimate gap fraction from both the hemispherical photos and the TLS POV-Ray simulation. Hemiphot calculates canopy gap fractions in 90 evenly sized concentric rings. To obtain the total gap fraction of an image:

$$G_{\text{tot}} = \sum_{\alpha=0.5}^{\alpha=89.5} (G_\alpha A_\alpha / A_{\text{tot}}) \tag{16}$$

Where G_α is the fraction of unfilled pixels in ring α, A_α is the sky area of the ring segment, and A_{tot} is the total sky area of the hemisphere.

We compared gap fraction estimates from both the TLS and hemispherical photo using a linear mixed model which accounted for variation among plots and between the two sites. While plots in Mtarure had a marginally steeper slope, this difference was not significant. We found that hemispherical photography almost exclusively over-estimated gap fraction, except in the most open subplots. Additionally, at lower gap fractions (greater canopy cover) the over-estimation of gap fraction by hemispherical photography was larger (Figure 5).

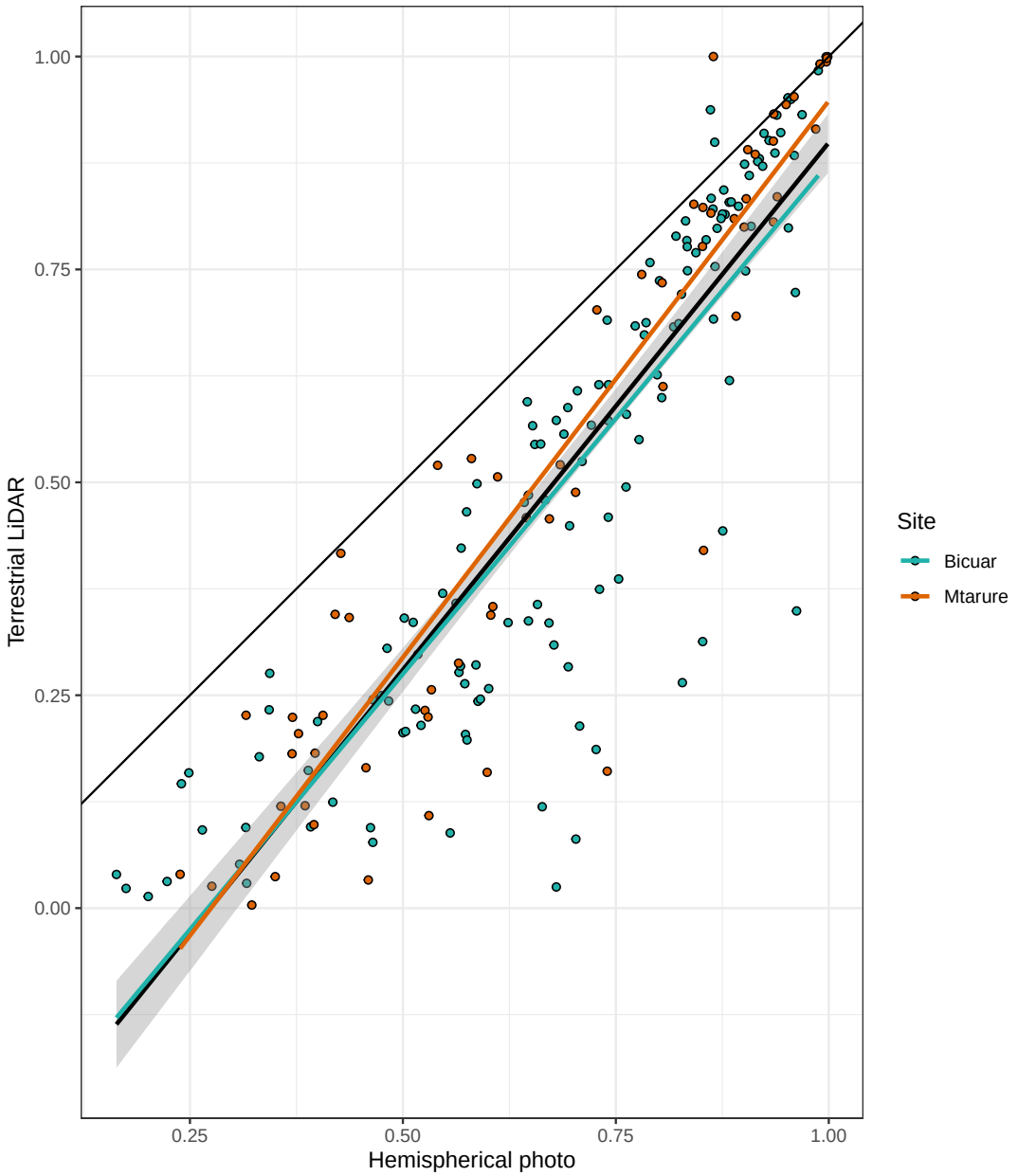

Figure 5: Comparison of gap fraction estimation from TLS and hemispherical photography. The black line of best fit is a linear model of all points ±1 standard error, while the coloured lines are site specific linear models.

4.4.3 Grassy biomass estimation

An allometric model was developed to estimate grassy biomass at every disc-pasture sample point using the grassy biomass sample masses. This model was only developed for Angola where grassy biomass samples were weighed. The model consisted of a linear mixed effects regression testing the relationship between disc-pasture height (independent) and grassy biomass (dependent), with a random slope term for each 1 ha plot.

Grassy volume was measured from TLS point cloud data following the methodology of. First the point cloud was cropped to points below 2 m. The point cloud was then aggregated to cubic voxels of 2 cm^3. Within each vertical 2 cm^2 column, the mean height of points was calculated, then

the volume below the mean was assumed to be entirely filled with grassy material.

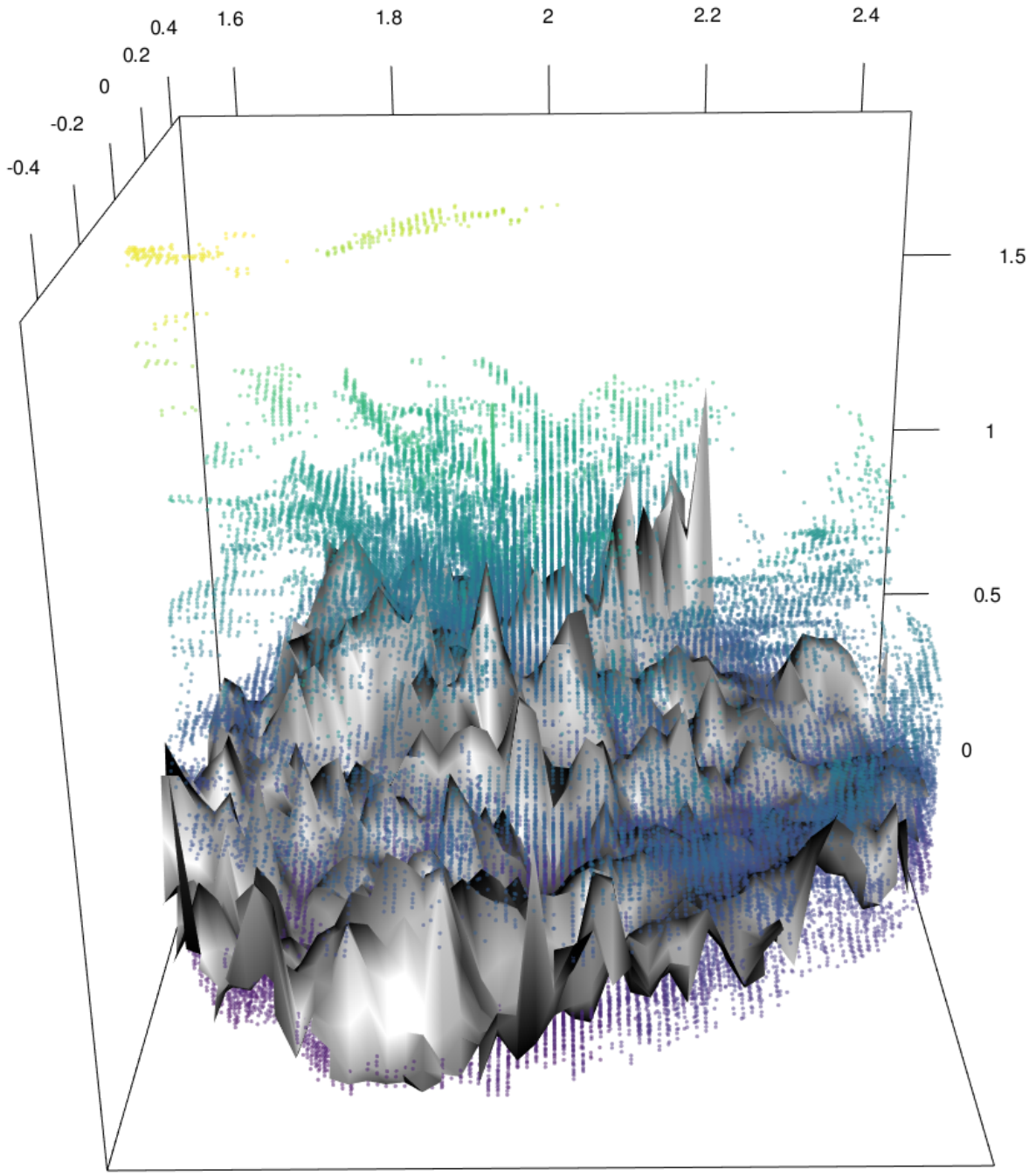

Figure 6: Point cloud with mean heights for each 2 cm^2 column labelled and the estimated grassy volume below.

4.4.4 Canopy rugosity

The canopy rugosity of each 1 ha plot was estimated. All scans from each plot were merged to a single point cloud, and noise reduction was performed as described above and the cloud was voxelised to 10 cm^3 cubic voxels. The point cloud was cropped to the plot boundaries, which were located with dGPS similar to the LiDAR targets.

A canopy height model was produced to describe the upper canopy surface. The 99th percentile of

height in each 10 cm^2 vertical column was extracted. The maximum height was not used as this occasionally constituted a severe outlier which skewed further canopy height model smoothing. We used the pit-filling algorithm described in Khosravipour et al. (2014) to smooth the canopy height profile by removing gaps within trees caused by incomplete penetration of the LiDAR beam.

From the canopy height profile we extracted a number of statistics for use in statistical modelling. We calculated the mean and coefficient of variation of canopy height across the plot (canopy rugosity), following (Parker and Russ, 2004). We calculated the Topographic Ruggedness Index (TRI) as the mean of absolute differences between the heights of each column and the height of its eight surrounding cells (Wilson et al., 2007). From this we estimated the plot level mean TRI and coefficient of variation.

We also calculated a second measure of canopy rugosity (R_c) following Hardiman et al. (2011), using all point cloud data rather than just the top surface:

$$R_c = \sigma(\sigma G_z)_x \tag{17}$$

Where G_z is the vertical height axis z, x is the horizontal axis, and σ is the standard deviation.

5 Statistical analysis

All linear mixed effects models werre conducted using the `{lmer}` package in R version 4.0.2 (R Core Team, 2020).

5.1 Foliage density profiles

We conducted a number of linear mixed effects models to assess the effects of tree diversity and stand structure on various aspects of canopy structure. Linear mixed effects models were used to account for the nested sampling structure of subplots within plots, and plots within sites.

For each subplot canopy structure measure, we created a linear mixed effects model with fixed effects for subplot species richness, stem density, and tree spatial structure.

5.2 Canopy gap fraction

We conducted a linear mixed effects model to assess the fit between gap fraction estimates from hemispherical photos and the hemispherical photo simulation produced from the TLS data. We included random slope terms for each 1 ha nested within site.

5.3 Grassy biomass

To estimate the correlation between grassy volume estimated by TLS and grass biomass estimated from the allometry of DPM height and grassy biomass samples, we conducted a linear mixed effects model of grass biomass vs. grassy volume, with nested random slope terms for each 1 ha plot nested within site.

We conducted a linear mixed effects model to assess the effects of canopy structure on grassy volume, with random slope terms for each 1 ha plot nested within site. We began with a maximal model which included subplot tree species richness, stem density, TLS gap fraction, layer diversity, height of maximum foliage density, standard deviation of the foliage density profile, and our simple measure of foliage density uniformity. We re-fitted the model with all possible combinations of fixed and random effects and compared AIC, BIC, and log-likelihood to determine which combination of explanatory variables best accounted for variation in grassy volume. Once this 'best model' had been identified we extracted effect sizes for each fixed effect as standardized slopes. We also compared random effects for each fixed effect to understand how the two sites differed.

5.4 Canopy rugosity

To understand the effect of species composition and stand structure on whole-plot canopy rugosity, we conducted a linear mixed effects model with fixed effects for the shannon diversity index of tree species diversity, stem density, and the coefficient of variation of stem diameter, with random intercept terms for each site.

We extracted slopes for each fixed effect to compare their effect sizes and compared our model with a null model which consisted only of the random effect of site and the fixed effect of stem density.

References

Bransby, D.I. and N.M. Tainton (1977). "The disc pasture meter : Possible applications in grazing management". In: *Proceedings of the Annual Congresses of the Grassland Society of Southern Africa* 12.1, pp. 115–118. DOI: 10.1080/00725560.1977.9648818.

Brusa, A. and D. E. Bunker (2014). "Increasing the precision of canopy closure estimates from hemispherical photography: Blue channel analysis and under-exposure". In: *Agricultural and Forest Meteorology* 195-196, pp. 102–107. DOI: 10.1016/j.agrformet.2014.05.001.

Chave, J. et al. (2014). "Improved allometric models to estimate the aboveground biomass of tropical trees". In: *Global Change Biology* 20.10, pp. 3177–3190. DOI: http://dx.doi.org/10.1111/gcb.12629.

Chen, X. et al. (Sept. 2011). *Trimble RTX, an innovative new approach for network RTK*. Tech. rep. Portland OR, USA: International Technical Meeting of the Satellite Division of the Institute of Navigation, ION GNSS, pp. 2214–2219.

Ehbrecht, Martin et al. (2016). "Effective number of layers: A new measure for quantifying three-dimensional stand structure based on sampling with terrestrial LiDAR". In: *Forest Ecology and Management* 380, pp. 212–223. DOI: 10.1016/j.foreco.2016.09.003.

Frazer, Gordon W. et al. (Sept. 2001). "A comparison of digital and film fisheye photography for analysis of forest canopy structure and gap light transmission". In: *Agricultural and Forest Meteorology* 109.4, pp. 249–263. DOI: 10.1016/s0168-1923(01)00274-x. URL: https://doi.org/10.1016%2Fs0168-1923%2801%2900274-x.

Hardiman, Brady S et al. (2011). "The role of canopy structural complexity in wood net primary production of a maturing northern deciduous forest". In: *Ecology* 92.9, pp. 1818–1827. DOI: 10.1890/10-2192.1.

Hu, Lile and Jiaojun Zhu (May 2009). "Determination of the tridimensional shape of canopy gaps using two hemispherical photographs". In: *Agricultural and Forest Meteorology* 149.5, pp. 862–872. DOI: 10.1016/j.agrformet.2008.11.008. URL: https://doi.org/10.1016%2Fj.agrformet.2008.11.008.

Khosravipour, Anahita et al. (2014). "Generating Pit-free Canopy Height Models from Airborne Lidar". In: *Photogrammetric Engineering & Remote Sensing* 80.9, pp. 863–872. DOI: 10.14358/pers.80.9.863.

Parker, Geoffrey G and Mary E Russ (2004). "The canopy surface and stand development: assessing forest canopy structure and complexity with near-surface altimetry". In: *Forest Ecology and Management* 189.1-3, pp. 307–315. DOI: 10.1016/j.foreco.2003.09.001.

R Core Team (2020). *R: A Language and Environment for Statistical Computing*. R Foundation for Statistical Computing. Vienna, Austria. URL: https://www.R-project.org/.

Rusu, Radu Bogdan et al. (2008). "Towards 3D Point cloud based object maps for household environments". In: *Robotics and Autonomous Systems* 56.11, pp. 927–941. DOI: 10.1016/j.robot.2008.08.005.

Spurr, S. H. (1962). "A measure of point density". In: *Forest Science* 8.1, pp. 85–96. DOI: http://dx.doi.org/10.1093/forestscience/8.1.85.

von Gadow, K. and G. Hui (2002). *Characterising forest spatial structure and diversity*. Ed. by L. Bjoerk. Lund, Sweden, pp. 20–30.

Wilson, Margaret F. J. et al. (2007). "Multiscale Terrain Analysis of Multibeam Bathymetry Data for Habitat Mapping on the Continental Slope". In: *Marine Geodesy* 30.1-2, pp. 3–35. DOI: 10.1080/01490410701295962.

Zhang, Keqi et al. (2003). "A progressive morphological filter for removing nonground measurements from airborne LIDAR data". In: *IEEE Transactions on Geoscience and Remote Sensing* 41.4, pp. 872–882. DOI: 10.1109/tgrs.2003.810682.